scientific reports

Check for updates

OPEN

Early-life exposure to 27.5 GHz 5G millimeter-wave radiation induces skin-related biological responses in mice

Francesca Palone[1,5], Emiliano Fratini[1,5], Flavia Novelli[1], Simona Leonardi[1], Ilaria De Stefano[1], Emanuela Pasquali[1], Mirella Tanori[1], Rosanna Pinto[1], Lucia Ardoino[1], Alessandro Zambotti[1], Francesca Camera[1], Marta Piscitelli[1], Caterina Merla[1], Simonetta Pazzaglia[1], Myles Capstick[2], Theodoros Samaras[3,4] & Mariateresa Mancuso[1]✉

The global rollout of 5G networks has raised questions regarding the potential biological effects of millimeter-wave exposure, particularly in the skin due to its limited penetration depth. This study examined the effects of whole-body exposure to 27.5 GHz millimeter waves, a frequency within the 5G FR2 bands, on skin-related biological responses in early life mice. *Patched1*- heterozygous knockout and wild-type CD1 mice were exposed from birth to weaning (P21), 23 h per day, in 10-minute ON/5-minute OFF cycles, at two power densities (6.67 and 20 W/m²). SHAM-exposed animals served as a control. No overt histological abnormalities were observed in exposed skin. However, molecular analyses revealed significant modulation of inflammation-related gene expression. Notably, *Ccl4*, *Csf2*, and *Tnfsf11* emerged as central regulatory nodes, displaying high degree and betweenness centrality across all groups, irrespective of genotype and sex. Crucially, exposure significantly stimulated mast cell degranulation and, in wild-type mice, led to a reduction in cutaneous glutamate levels. Concurrently, a down-regulation of transcripts associated with cutaneous sensory components (*Calca*, *Mrgprd*) was observed within the skin microenvironment. These findings show that 27.5 GHz exposure induces coordinated changes in cutaneous inflammatory pathways and mast cell-mediated homeostasis without detectable structural damage. Overall, these results demonstrate a localized molecular and cellular response within the cutaneous microenvironment, reflecting a subtle homeostatic shift, and suggest that genetic background may contribute to variability in the biological response to millimeter-wave exposure.

Keywords *Ptch1*$^{+/-}$ mice, MMW, Inflammation, Mast cells, Radiofrequency radiation

The introduction of fifth-generation (5G) radiofrequency (RF) radiation technology marks a significant advancement in mobile communication, offering ultra-high speeds and low latencies. These performances are made possible by using the millimeter wave (MMW) spectrum. Among the available bands, 3GPP band n258 (called 26 GHz) covers frequencies from 24.25 to 27.5 GHz, while 3GPP band n257 (widely known as 28 GHz) spans from 26.5 to 29.5 GHz. Currently, the 26 GHz band is the top priority for the mobile industry, receiving the most significant support. However, the growing global demand for 5G is also driving interest in additional frequency bands, including the 28 GHz band, to expand capacity and meet market requirements.

The global rollout of 5G technology is proceeding without comprehensive studies on its potential risks to human health and the environment[1]. This has sparked widespread debate and concern among individuals in many countries[2].

A significant concern among some future users is the proximity of both antennas and devices to the human body. This proximity means that the skin and eyes, the primary areas exposed to MMW due to its micrometric

[1]Division of Biotechnologies, Casaccia Research Center, Italian National Agency for New Technologies, Energy and Sustainable Economic Development (ENEA), Rome 00123, Italy. [2]Foundation for Research on Information Technologies in Society (IT'IS), Zurich 8004, Switzerland. [3]CIRI – Center for Interdisciplinary Research and Innovation, Aristotle University of Thessaloniki, Thermi 57001, Greece. [4]Radiocommunications Lab, Department of Physics, Aristotle University of Thessaloniki, Thessaloniki 54124, Greece. [5]Francesca Palone and Emiliano Fratini contributed equally to this work. ✉email: mariateresa.mancuso@enea.it

penetration depth, are at the forefront of potential risks. Despite these concerns, the current body of scientific research on the biological effects of MMW remains limited. Only around 99 studies (reviewed in[3]) have explored their impact on skin and skin cells, highlighting a lack of sufficient evidence to establish comprehensive, science-based exposure limits or health policies. Given this gap, it is evident that more high-quality research is needed to determine whether MMW exposure poses a health risk.

The SEAWave project (https://seawave-project.eu) aims to provide new scientific data to evaluate the potential health risks associated with exposure to 5G frequency bands, particularly those in the FR2 spectrum, such as 27.5 GHz (within the aforementioned bands). The project investigates and assesses the effects of such exposure from the early life stage through to adulthood, as different age groups may exhibit varying sensitivities due to the distinct physiological characteristics of the organisms studied at each developmental stage.

A key focus of the project is assessing the potential co-carcinogenic effects of prolonged skin exposure to this frequency. To achieve this result, *Patched1* heterozygous knockout (*Ptch1*$^{+/-}$) mice served as a significant model for studying basal cell carcinoma (BCC), a common type of skin cancer associated with mutations in the Hedgehog signalling pathway, as well as other tumors like medulloblastomas and rhabdomyosarcoma[4]. Past studies showed that these mice develop skin tumors resembling human BCC after exposure to environmental stressors such as ultraviolet (UV)[5] or ionizing radiation[6] replicating the disease's pathology and genetic underpinnings as in humans. Notably, early-life exposure of mice to stressors during critical phases of the hair growth cycle, such as the first anagen phase[7] results in a significantly higher incidence of BCC compared to other phases, including telogen (resting phase).

The SEAWave approach is driven by growing concerns about the increased vulnerability in the early phases of life to electromagnetic fields. During the first 21 days of life, early life mice possess thinner skin, developing organs, and immature immune systems, which may increase their sensitivity to electromagnetic radiation. This makes them a critical subject for study in order to better understand the risks associated with 5G FR2 exposure across different stages of development.

Thus, in this paper, we first focused on the skin analysis of *Ptch1*$^{+/-}$ mice and their wildtype CD1 counterparts, whole-body exposed from birth to weaning (for a total of 21 days) at 27.5 GHz, 10 min on and 5 min off, for 23 h per day at two power densities (6.67 and 20 W/m²). A SHAM exposed group, in which no signal was delivered to the animals, was included as a control. Particular attention has been given to characterizing potential inflammatory processes triggered by 5G exposure at 27. 5 GHz in the skin of *Ptch1*$^{+/-}$ mice, because a complex interplay of immune cells, cytokines, chemokines, and growth factors can ultimately drive genetic and epigenetic changes in skin cells, fostering a malignant transformation. Furthermore, the modulation of local cutaneous sensory markers (*Calca* and *Mrgprd*) was evaluated, as these genes are intimately linked to tissue homeostasis. Cutaneous sensory components not only respond to local microenvironmental changes but also play a pivotal role in modulating regional tissue responses. Local cellular processes can shift the expression of these markers, while alterations in the cutaneous microenvironment can, in turn, influence resident cell activity[8–10]. In this context, we also investigated the modulation of cutaneous glutamate, a key signalling molecule that mediates communication within the dermal microenvironment, modulates mast cell activity, and interacts with localized inflammatory pathways, potentially influencing the local tissue environment[11,12]. The results obtained in this first study on early life animals, supported by an accurate murine skin dosimetry based on experimental measurements of skin layer thicknesses during the first hair growth cycle occurring within the 21-day exposure period[13], indicate activation of inflammatory processes in the skin of animals exposed to 27.5 GHz during early life stages. These effects were accompanied by changes potentially consistent with local mast cell network and signalling components, including modifications in glutamate levels. These findings suggest that exposure to MMW during the early stages of life may be associated with subtle homeostatic alterations within the skin microenvironment, independently of genotype or gender. This concern arises from the critical role inflammation plays in promoting the clonal expansion of mutated cells, which can lead to malignancies. Inflammatory processes can create a microenvironment that facilitates the proliferation and survival of mutated cells, increasing the likelihood of their progression to cancer. The observed molecular changes further support a localized modulation of skin homeostasis following 27.5 GHz exposure. Early-life exposure, during a period of heightened developmental sensitivity, may influence these responses due to immature immune regulation and increased cellular vulnerability.

Results

Exposure parameters

The exposure system comprises three reverberation chambers providing high power density (HPD, 20 W/m²), low power density (LPD, 6.67 W/m²) and SHAM exposure (Fig. 1).

The choice of power density levels is based on exposing one group to a level above the ICNIRP 2020 general-public reference level for 6–300 GHz (10 W/m² at 27.5 GHz) and another group to a level below this threshold, with HPD at 20 W/m², and LPD at 6.7 W/m² (ICNIRP 2020). These power density values are determined by the reverberating chamber amplification chains, which only allow specific output power levels. Therefore, these outputs are fixed and not adjustable. This design was necessary to contain the high costs of the system operating at millimeter frequency. It is important to note that both exposure ranges (HPD and LPD) are below the levels that would cause thermal effects in the exposed targets, placing them in the "non-thermal" range.

Electromagnetic reverberation chambers were used to expose the animals at a frequency of 27.5 GHz representative of high-band 5G frequencies (25–39 GHz). Over the 21 days of the study, the incident power densities, during the 10-minute ON periods, were for the HPD 20.0 W/m² with 3.8% standard deviation (SD) and LPD 6.72 W/m² with 4.4% SD. In the SHAM chamber, the exposure was 0 W/m². Intermittent exposure was chosen to simulate a more realistic exposure scenario, where the signal is not always on. However, a consistent percentage of "on" time was considered to represent a strong exposure modality.



Fig. 1. Exposure system. From left to right: **(1)** view of the three reverberation chambers; **(2)** interior view of an empty chamber showing metal model stirrers; and **(3)** a chamber equipped with standard mouse cages.

Exposures were at the planned levels with no deviations or periods where planned exposures did not occur. The temperatures in the three chambers were within 0.3 °C of each other with an average of 19.3 °C, the chambers had slightly different temperature variations with SDs of 0.60 °C for HPD, 0.50 °C for LPD and 0.41 °C for SHAM, these fluctuations be equated to the power dissipated in each chamber in mice bedding and food.

Overall health condition of the animals at the end of exposure

All the mice included in the experiment survived for the full 21 days of exposure to 27.5 GHz at both power densities tested without any signs of distress or illness. No significant alterations in normal growth patterns were observed during the early life exposure. There were no delays in eye opening, changes in hair growth, or signs of skin dryness. The pups showed typical development, with no deviations from expected milestones in behaviour or physical condition. Body weights were recorded from pups at the end of exposure (P21), and no significant differences were observed between SHAM, LPD, and HPD groups, in either WT or *Ptch1*$^{+|-}$ mice (Supplementary Figure S1).

Histopathology of the skin in response to 27.5 GHz exposure

Fields incident on the skin of the mice at 27.5 GHz result in both reflection and transmission at the air-skin boundary, the transmitted wave is rapidly adsorbed by the superficial skin layers leading to the highest exposure being in these layers[14], hence, we looked for alterations in the dorsal skin of the 21-day exposed animals. Histological analysis of the dorsal skin did not show any evident alterations in the skin structure of WT and *Ptch1*$^{+/-}$ mice, both in LPD and in HPD groups. No significant differences in hair cycle phase were observed between the SHAM, LPD, and HPD groups, both in WT and in *Ptch1*$^{+/-}$ mice. The skin appeared to be in the late catagen/telogen phase in all groups (Fig. 2A), consistent with the normal hair growth curve at P21[12]. Quantitative morphometric analyses confirmed no significant differences in epidermal thickness, hair follicle density, or follicle depth across exposure conditions or genotypes (Fig. 2B). Hair follicle density and depth values were comparable among groups and consistent with an early anagen phase, indicating preserved follicular growth dynamics. Similarly, dermal cellularity was unchanged, and immunohistochemical analysis of F4/80 (Fig. 2C, Supplementary Fig. 2) showed no differences in macrophage infiltration between groups.

Overall, 27.5 GHz exposure did not induce detectable structural changes or inflammatory cell recruitment in dorsal skin under the experimental conditions tested.

Exposure to 27.5 GHz during the early life stages induces dysregulation of skin genes involved in inflammatory processes

In the absence of histological abnormalities in the skin after 5G exposure, we investigated potential molecular alterations in the inflammatory process in *Ptch1*$^{+/-}$ mice. This approach was motivated by the ability of keratinocytes and other resident skin cells to produce cytokines and chemokines, thereby contributing to tissue-level inflammatory signatures independently of overt immune cell infiltration. Gene expression profiling using targeted qPCR arrays covering 84 inflammation-related genes was performed. Differentially expressed genes were identified using fold change thresholds (FC ≥ 2) and statistical significance ($p < 0.05$), revealing distinct sex-specific patterns of inflammatory gene regulation. The heatmaps shown in Fig. 3A illustrate the magnitude of gene expression, with colours ranging from green to red, in the comparison between the LPD and HPD experimental groups versus the SHAM group.

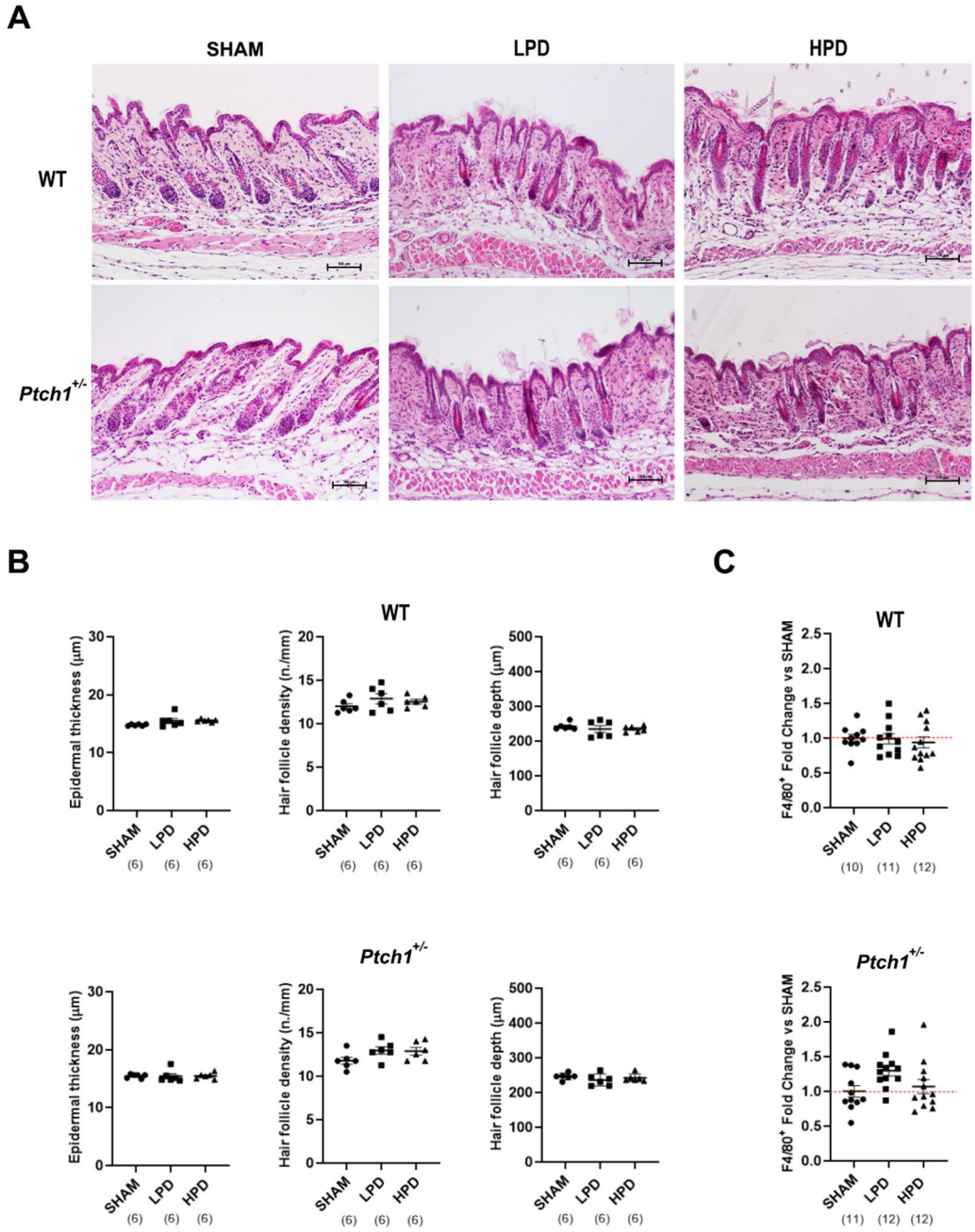


Fig. 2. Histological and morphometric analysis of dorsal skin following 5G exposure. **(A)** Representative images of dorsal skin sections at P21 after H&E staining. No evident skin alterations across SHAM, LPD, and HPD groups were evidenced, regardless of genotype. Magnification: 10x. Scale bar: 100 µm. **(B)** Morphometric analysis of skin architecture. Graphs show epidermal thickness (µm), hair follicle density (number of follicles per mm of skin), and hair follicle depth (µm), used to assess potential radiation-induced structural and functional changes in WT and *Ptch1*$^{+/-}$ mice. **(C)** Quantification of F4/80^{+} macrophage infiltration. Automated digital image analysis was performed using HistoQuest software (TissueGnostics). Macrophage density is expressed as fold change relative to the respective SHAM controls, for each genotype. The number of animals analyzed is indicated in parentheses below the x-axis of each dot plot. Data are presented as mean ± SEM. Statistical analysis was performed using the Mann-Whitney U test (comparisons: SHAM vs. LPD; SHAM vs. HPD).

Network analysis of differentially expressed genes in Fig. 3B shows the interaction of upregulated (red) and downregulated (blue) genes based on STRING protein-protein interaction database.

In detail, in *Ptch1*$^{+/-}$ males, the RT2 Profiler PCR Array revealed that 21 out of 84 genes were significantly modulated, 5 of which were modulated in both the LPD and HPD groups (*Ccl4*, *Ccr6*, *Csf2*, *Il10ra*, *Tnfsf11*), and the other 16 genes were deregulated only at HPD. In *Ptch1*$^{+/-}$ females, 13 out of 84 genes were significantly

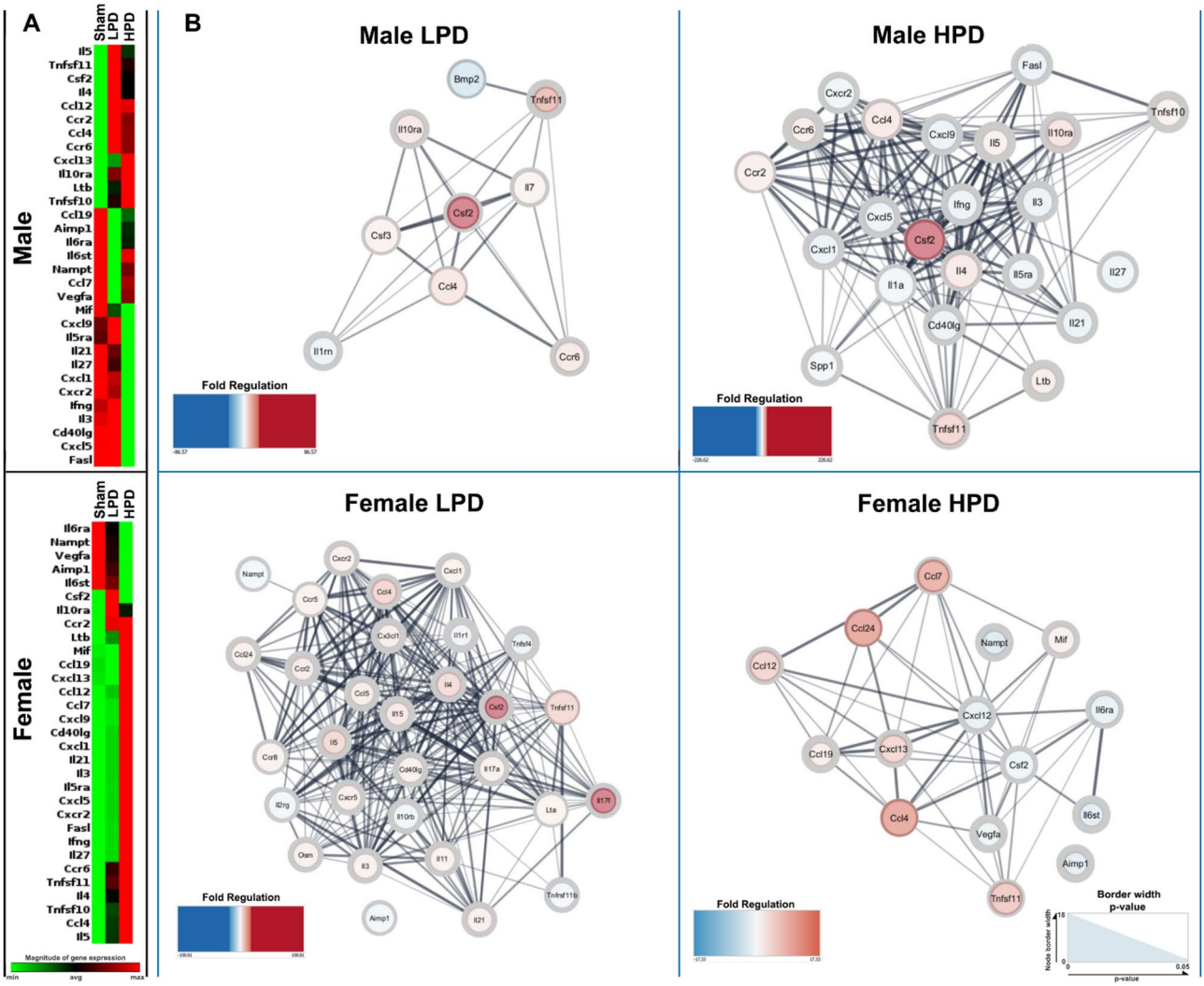


Fig. 3. Gene expression profiling and network analysis in male (upper panel) and female (lower panel) mice. **(A)** The heatmaps display the relative expression levels of each gene included in the RT² Profiler PCR array. Gene expression values are represented on a continuous color scale, where green indicates lower expression, black represents average expression, and red denotes higher expression relative to the dataset mean. Each row corresponds to a single gene, and the color intensity reflects the magnitude of up- or down-regulation. This visualization enables rapid identification of expression patterns and highlights genes that are markedly over- or under-expressed across the analyzed samples. **(B)** Network diagram of deregulated genes based on STRING protein–protein interaction database. Node fill colours represent the direction and magnitude of gene regulation (red: upregulated; blue: downregulated), while border thickness indicates statistical significance (thicker borders correspond to lower p-values, meaning higher statistical significance; p-value range: 0 to 0.05), relative to SHAM groups. Three pools of three animals each (biological replicates) for each sex, were analysed. Statistical significance was assessed using the unpaired t-test with Welch's correction on ΔCt values. Fold changes were calculated using the 2^-ΔΔCt method.

modulated, 5 of which were modulated in both the LPD and HPD groups (*Aimp1*, *Ccl4*, *Csf2*, *Nampt*, *Tnfsf11*) and the other 8 genes were deregulated only at HPD. The raw microarray dataset obtained from *Ptch1*$^{+/-}$ female and male mice is available in Supplementary Table S1.

The Reactome Pathway Enrichment Analysis (Supplementary Figure S3) showed a different modulation of pathways between male and female groups. Defensins, particularly β-Defensins, were identified as overrepresented pathways shared by both treatments (LPD and HPD) in male groups. In contrast, pathways related to the metabolism of vitamins and cofactors, specifically nicotinate metabolism and nicotinamide salvaging, were common to both LPD and HPD female groups. Furthermore, MAPK family signalling cascades, including MAPK1/MAPK3 signalling, were overrepresented across all groups, irrespective of gender. Notably, network analysis revealed *Ccl4*, *Csf2*, and *Tnfsf11* as central nodes, exhibiting high degree and betweenness centrality in all groups (Supplementary Figure S4). Focusing on genes altered at both power densities and in both sexes, RT-PCR validation was performed in all *Ptch1*$^{+/-}$ exposed mice ($n = 71$; 21 SHAM, 25 LPD, and 25 HPD,

with equal distribution between males and females). Furthermore, to assess generalizability beyond genotype, a representative cohort of WT animals (3 per group) was also evaluated. According to data derived from array analysis, the expression levels of *Ccl4*, *Csf2*, and *Tnfsf11* were significantly increased both in *Ptch1*$^{+/-}$ and WT mice, regardless of sex and delivered power densities (Fig. 4).

Overall, molecular analyses following early life 27.5 GHz exposure revealed a measurable dysregulation of inflammation-associated gene expression at both power densities, with similar directionality across genotypes.

Modulation of local neuro-immune transcripts following 27.5 GHz exposure

In response to early life 27.5 GHz exposure gene expression analysis was performed on skin transcripts known to be associated with peripheral nerve terminals, *Cgrpα* (gene *Calca*) and *MrgprD* (gene *Mrgprd*), which serve as markers for peptidergic and non-peptidergic subpopulations within the skin microenvironment, respectively. These markers are tipically associated with superficial skin innervations involved in the perception of itch, cutaneous pain, and stress. RT-PCR analysis was conducted on dorsal skin samples from both *Ptch1*$^{+/-}$ mice ($n = 71$; 21 SHAM, 25 LPD, and 25 HPD, equally distributed between sexes) and WT mice ($n = 67$; 25 SHAM, 22 LPD, and 20 HPD, also balanced between sexes). At the whole-tissue level, WT mice showed a significant decrease in both *Calca* and *Mrgprd* expression levels, except for *MrgprD* in males, which did the not reach statistical significance (Fig. 5). In *Ptch1*$^{+/-}$ mice, a similar significant decrease was observed for *Calca* in both sexes, whereas *MrgprD* downregulation did not reach statistical significance. Consistent with the whole-skin

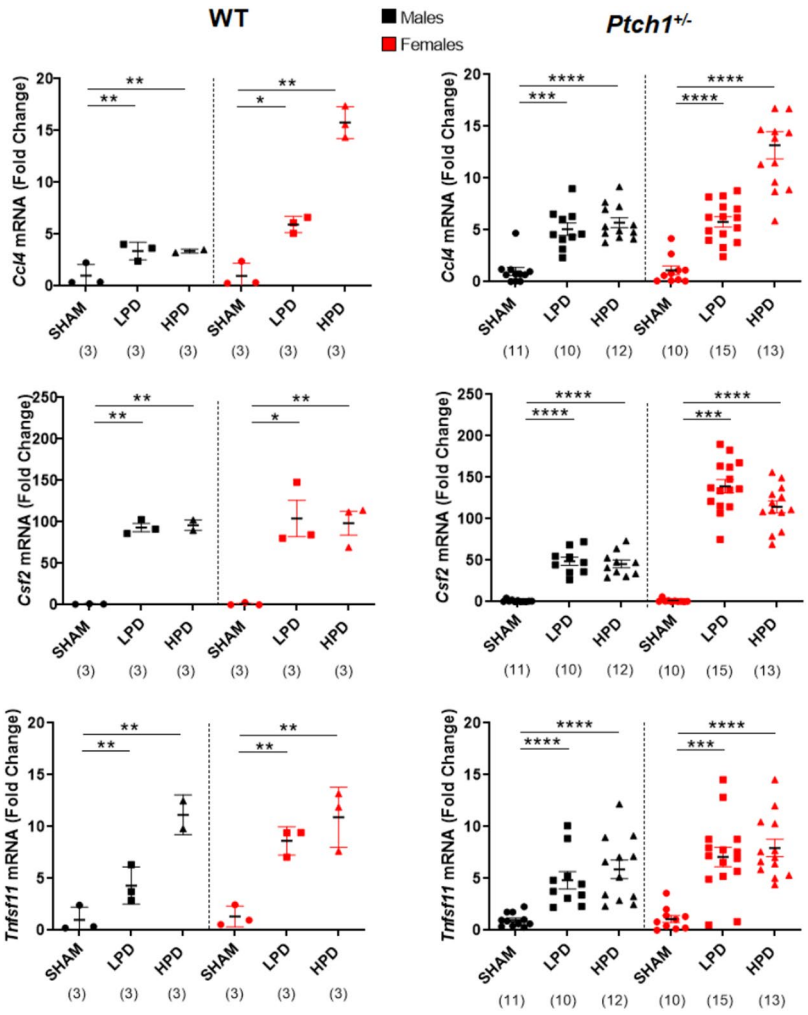


Fig. 4. qPCR analysis of inflammatory gene expression in the skin of *Ptch1*$^{+/-}$ and WT. mice. Quantitative PCR analysis of *Ccl4*, *Csf2*, and *Tnfsf11* expression in skin samples from *Ptch1*$^{+/-}$ and WT mice. Results are presented as fold change (mean ± S.E.M.) relative to the SHAM group, comparing mice on LPD and HPD conditions. The number of animals per group is indicated in brackets below the x-axis, WT male: SHAM (3), LPD (3), HPD (3); WT female: SHAM (3), LPD (3), HPD (3); Ptch1$^{+/-}$ male: SHAM (11), LPD (10), HPD (12); Ptch1$^{+/-}$ female: SHAM (10), LPD (15), HPD (13). Comparison among groups was performed using the nonparametric Kruskal–Wallis test followed by Dunn's multiple comparisons test. $p < 0.05$ (*), $p < 0.01$ (**), $p < 0.001$ (***), $p < 0.0001$ (****) relative to the respective SHAM group.

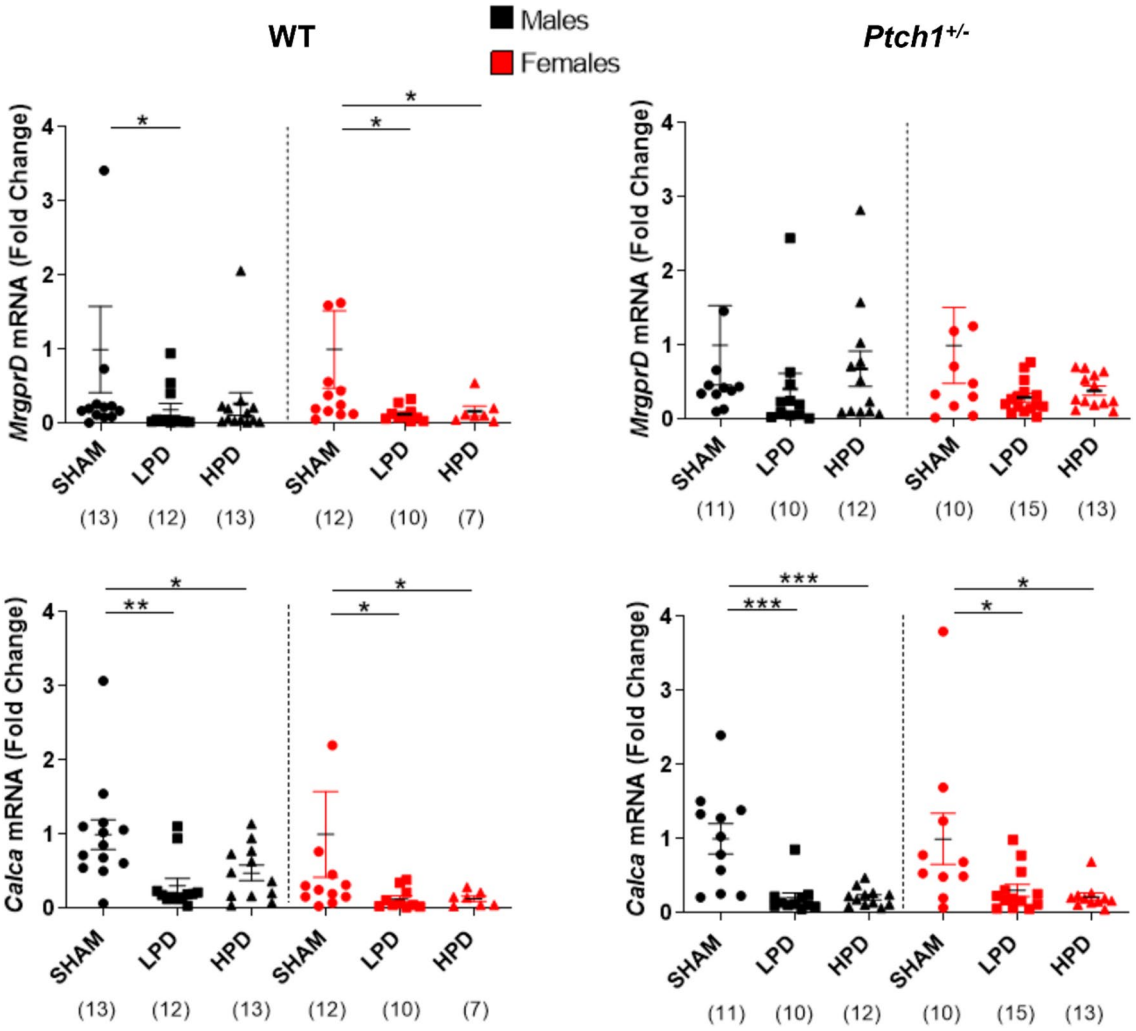


Fig. 5. qPCR analysis of *MrgprD* and *CGRPα* gene expression in the skin of *Ptch1*$^{+/-}$ and WT mice. Quantitative PCR analysis of *MrgprD* and *CGRPα* expression in skin samples from *Ptch1*$^{+/-}$ and WT mice. Results are shown as fold-change (mean ± S.E.M.) relative to the SHAM group, comparing LPD and HPD conditions. The number of animals per group is indicated in brackets below the x-axis, WT male: SHAM (13), LPD (12), HPD (13); WT female: SHAM(12), LPD (10), HPD (7); Ptch1$^{+/-}$ male: SHAM (11), LPD (10), HPD (12); Ptch1$^{+/-}$ female: SHAM (10), LPD (15), HPD (13). Statistical significance among groups was determined using Kruskall-Wallis test with Dunn's Multiple Comparison post test. $p < 0.05$ (*), $p < 0.01$ (**),$p < 0.001$ (***) relative to the respective SHAM group.

sampling approach, these transcriptional shifts reflect a localized molecular modulation within the cutaneous environment rather than definitive alterations in functional nociceptor activity.

Cutaneous glutamate levels in WT and *Ptch1*$^{+/-}$ mice after 27.5 GHz exposure

To further characterize the biochemical microenvironment of the exposed skin, we quantified glutamate levels as an indicator of peripheral neuro-immune signalling. In WT mice, SHAM-exposed animals exhibited basal glutamate levels of 2.86 ± 0.15 µM/mg tissue, which were reduced following 27.5 GHz exposure in both LPD ($p < 0.0001$) and HPD ($p < 0.05$) groups (Fig. 6). This reduction was observed alongside decreased expression of nociceptive markers *(Calca*, *Mrgprd)* in the same groups.

In contrast, *Ptch1*$^{+/-}$ mice showed lower basal glutamate levels compared to WT animals ($p < 0.001$), with no significant changes following exposure at either power density.

Overall, glutamate levels differed between genotypes, with exposure-related reductions observed in WT mice and a stable profile in *Ptch1*+/- animals.

Mast cell degranulation

In vivo evidence supports a strong functional relationship between mast cells and nociceptors, highlighting how this neuroimmune interaction plays a key role in the regulation of pain, inflammation and itch[15]. In addition, mast cells act as critical crucial effector cells in inflammatory responses through the release of bioactive mediators

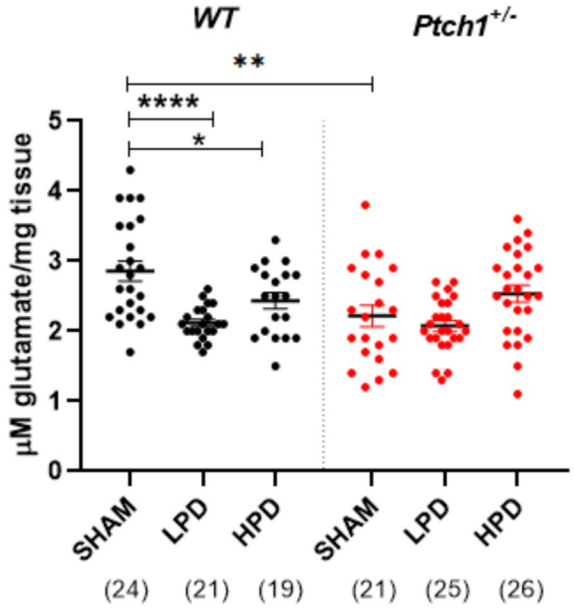


Fig. 6. Quantification of cutaneous glutamate levels in WT and *Ptch1*$^{+/-}$ mice exposed to 27.5 GHz. Glutamate concentrations were measured and normalized to tissue weight (µM/mg of tissue). Data are presented as individual points and the number of animals per group is indicated in parentheses below the x-axis. Statistical comparisons were performed against the respective SHAM control group for both WT *and Ptch1*$^{+/-}$ genotypes using an unpaired t-test with Welch's correction. $p < 0.05$ (*), $p < 0.01$ (**), and $p < 0.0001$ (****).

via degranulation[16]. We therefore assessed mast cell distribution and activation status in dermal skin sections using toluidine blue staining. As shown in Fig. 7, total mast cell density per unit area did not differ between genotypes or experimental groups. These changes are consistent with the significant upregulation of *Csf2* gene expression found in the exposed skin samples (Table 1A and B). In contrast, the proportion of degranulated mast cells was significantly increased in exposed animals across both genotypes.

Overall, these data indicate that 27.5 GHz exposure is associated with increased mast cell degranulation without affecting mast cell density.

Discussion

The effects of RF radiation on biological systems have been extensively investigated due to the widespread use of wireless technologies. The primary established effect remains thermal, leading to tissue heating; under current ICNIRP guidelines, predicted temperature increases associated with 5G exposures remain well below thresholds for tissue damage and are considered of low physiological relevance[13,17,18]. No consistent evidence of RF-induced dermatological pathology has been demonstrated under regulated exposure conditions. Available evidence suggests that biological responses in the 26–30 GHz range are driven primarily by power density and thermal load rather than carrier frequency specificity[19]. Millimeter-wave exposure above 10 GHz is largely confined to superficial skin layers due to limited tissue penetration[17].

In the present work, we investigated the effects of continuous 5G whole-body exposure at 27.5 GHz in *Ptch1*$^{+/-}$ mice and their WT CD1 counterparts for 21 days from birth to weaning. The absence of mortality, distress, or developmental delays among pups exposed to 27.5 GHz at both low and high-power densities is an important initial observation. Early life growth patterns, including body weight, eye opening, and hair development, proceeded normally. This suggests that short-term exposure to 5G MMW at these intensities does not cause noticeable toxicity or growth impairment, consistent with previous assessments by the Scientific Committee on Emerging and Newly Identified Health Risks (SCENIHR)[20], which reports no conclusive evidence of adverse systemic effects of RF radiation under non-thermal exposure conditions.

Histological analysis revealed no structural alterations or immune cell infiltration in the skin, indicating preserved tissue architecture under both exposure conditions.

Despite the absence of histopathological changes, transcriptomic analyses revealed modulation of inflammatory and immune-related pathways, including sex-dependent enrichment of β-defensins in males and metabolic pathways such as nicotinate metabolism in females. Sex can influence cytokine profiles and immune-cell activation patterns after perturbation, providing a plausible framework for these findings[21,22]. These molecular shifts indicate a mild and sex-influenced transcriptional response, which should be interpreted as correlational signals of stress/inflammatory priming rather than evidence of overt inflammatory disease. Interestingly, MAPK signaling pathways, central hubs in transducing environmental stress[23,24], were enriched across all exposed groups regardless of sex. However, these transcriptional changes were not complemented by functional or protein-level validation, limiting the ability to infer downstream biological effects. Overall, these findings suggest a coordinated but weakly coupled transcriptional response to 27.5 GHz exposure.

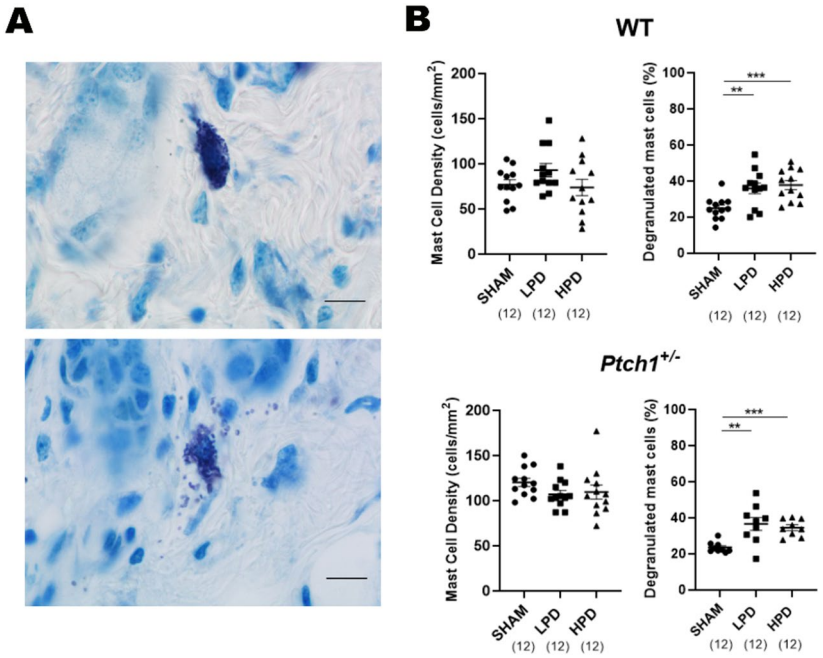


Fig. 7. Mast cell degranulation in the skin of *Ptch1*$^{+/-}$ and WT mice. **(A)** Representative Toluidine blue-stained skin sections showing mast cell morphology. The upper panel depicts an intact mast cell with densely packed cytoplasmic granules contained within a well-defined cellular boundary. The lower panel shows a degranulated mast cell, characterized by extensive dispersion of granules into the surrounding extracellular matrix. Magnification: 100x. Scale bar: 10 µm. **(B)** Quantitative analysis of mast cell density and degranulation in WT and *Ptch1*$^{+/-}$ mice following 5G exposure. Total mast cell counts were normalized to the analyzed tissue area (700,000 µm²). The degranulation index is expressed as the percentage of degranulated mast cells relative to the total mast cell count. Data are presented as mean ± SEM. Statistical significance was assessed using the Mann–Whitney U test. $p < 0.01$ (**), $p < 0.001$(***).

Lack of immune cell recruitment despite changes in inflammatory gene expression suggests an early or low-grade signaling state. Resident skin cells, such as keratinocytes, could act as primary "sensors" of MMW energy, producing cytokines and chemokines that create tissue-level inflammatory signatures without requiring frank immune cell recruitment.

Network analysis identified *Ccl4*, *Csf2*, and *Tnfsf11* as central nodes within immune-related signaling networks. *Ccl4* encodes a chemokine involved in macrophage recruitment and oxidative stress–associated inflammatory priming, with reported links to mast cell activation and degranulation[25,26]. *Csf2* regulates myeloid differentiation and supports mast cell activation, promoting the release of pro-inflammatory mediators such as histamine, TNF-α, IL-6, and prostaglandins[27–29]. *Tnfsf11* has likewise been implicated in enhancing mast cell degranulation[30–32]. The concurrent upregulation of these genes together with increased mast cell degranulation supports the presence of a coordinated activation of cutaneous immune signaling pathways rather than isolated transcriptional events.

In this context, changes in the cutaneous transcript levels of skin nociceptor-associated markers (*Calca* and *Mrgprd*) were observed following 27.5 GHz exposure. Although gene expression by RT-PCR in whole-skin cannot distinguish between a downregulation of gene expression per individual neuron as well as a reduced density of sensory terminals in the dermis, our results strictly reflect localized transcriptional shifts within the cutaneous microenvironment. Behavioral or electrophysiological data will be necessary to better understand a possible correlation with functional neuronal dysregulation or altered dorsal root ganglia (DRG) activity.

Biochemical analysis revealed genotype-dependent differences in cutaneous glutamate levels. Glutamate has been reported in peripheral tissues in the context of local cellular signaling[33,34]. WT mice showed a reduction following exposure, consistent with previous reports of modulation of peripheral excitatory signaling in cutaneous tissues[35,36]. In contrast, *Ptch1*$^{+/-}$ mice exhibited lower baseline levels and no exposure-related changes across conditions. Given the correlative nature of these measurements, these data do not support a causal role for glutamate in the observed responses. Instead, glutamate modulation may represent a secondary and context-dependent feature of the local tissue environment. Additional mechanisms may contribute to mast cell activation in this context, including established local inflammatory pathways[37], which will require further investigation.

Finally, mast cell analysis demonstrated increased degranulation without changes in cell density. Mast cells are recognized as key effector cells in inflammatory responses through the release of bioactive mediators upon degranulation[16]. In the present study, increased mast cell degranulation occurred in parallel with changes in selected immune-related gene expression; however, this response should be interpreted as a parallel immune activation event rather than evidence of a unified mechanistic pathway linking cellular, metabolic, and immune

Gene	Fold regulation LPD vs. SHAM	*p* value	Fold regulation HPD vs. SHAM	*p*-value
A) Ptch1$^{+/-}$ male mice				
Csf2	86.57	0.020795	42.79	0.044420
Tnfsf11	13.41	0.000754	8.05	0.019841
Il10ra	3.98	0.017068	4.98	0.010224
Ccl4	4.44	0.040614	3.69	0.040717
Il4	6.12	0.094020	3.62	0.030604
Ccr6	3.79	0.019721	3.18	0.000078
Ltb	1.90	0.183872	3.08	0.002192
Ccr2	3.15	0.179407	2.65	0.046165
Il5	4.76	0.063721	2.49	0.001555
Tnfsf10	1.79	0.099846	2.38	0.007420
Cxcr2	−1.10	0.918478	−2.29	0.022887
Il27	−1.28	0.946980	−2.46	0.032198
Il5ra	1.28	0.409955	−2.55	0.018550
Cd40lg	1.00	0.803673	−2.77	0.018300
Cxcl1	−1.08	0.897058	−2.77	0.018300
Cxcl5	1.01	0.796680	−2.77	0.018300
Cxcl9	1.26	0.436226	−2.77	0.018300
Fasl	1.01	0.796704	−2.77	0.018300
Ifng	1.09	0.675255	−2.77	0.018300
Il21	−1.23	0.997408	−2.77	0.018300
Il3	1.04	0.754625	−2.77	0.018300
B) Ptch1$^{+/-}$ female mice				
Csf2	*108.81*	*>0.000001*	*−2.23*	*0.044945*
Ccl4	*7.78*	*0.013637*	*18.55*	*0.082228*
Ccl7	*1.72*	*0.313217*	*16.38*	*0.051307*
Tnfsf11	*7.59*	*0.055292*	*10.92*	*0.053656*
Ccl12	*1.77*	*0.268292*	*8.43*	*0.041410*
Ccl19	*−1.14*	*0.560924*	*3.16*	*0.002132*
Mif	*−1.04*	*0.870014*	*2.29*	*0.027444*
Vegfa	*−1.34*	*0.218310*	*−2.50*	*0.005170*
Il6ra	*−1.53*	*0.180482*	*−3.24*	*0.041702*
Cxcl12	*−1.51*	*0.199569*	*−3.25*	*0.034195*
Aimp1	*−1.38*	*0.041043*	*−4.18*	*0.000147*
Il6st	*−1.26*	*0.072692*	*−4.41*	*0.000355*
Nampt	*−1.56*	*0.041475*	*−5.39*	*0.002161*

Table 1. List of the inflammatory pathway genes analysed in *Ptch1*$^{+/-}$ male (**A**) and female (**B**) mice.

compartments. Together, these data indicate that mast cell activation occurs within a broader but non-integrated cutaneous response to exposure.

Overall, 27.5 GHz exposure induced a mild and coordinated molecular response in the skin, characterized by transcriptional modulation of immune-related pathways and increased mast cell degranulation. These changes are best interpreted as a form of transient cutaneous stress or adaptive signaling rather than pathological inflammation. Remarkably, the similarity of effects across both LPD and HPD conditions, despite HPD exceeding the ICNIRP general public limit (10 W/m^2)[17], suggests that even exposures within or near regulatory limits may elicit subtle biological signaling in young skin. The restriction to a single postnatal time point (P21) further limits conclusions regarding the persistence or reversibility of these effects.

In summary, exposure to 5G frequency at 27.5 GHz did not induce overt structural, histological, or cellular alterations in young mouse skin, while molecular changes were limited to a mild activation of immune-related pathways without evidence of tissue-level pathology. Glutamate alterations, although genotype-dependent, were not consistently associated with transcriptional or functional outcomes, further supporting their interpretation as secondary and context-dependent changes within the local tissue environment rather than mechanistically causal events. Lastly, the observed changes in transcripts associated with cutaneous sensory components further support a localized homeostatic shift. Therefore, these findings should be considered strictly illustrative of early-stage, localized tissue insights within a specific developmental window. Future independent investigations utilizing standalone longitudinal designs focusing on broader systemic effects will be necessary to explore different experimental timelines or prospective homeostatic adaptations.

Materials and methods

Exposure system

5G signals were synthesized at 2 GHz then upconverted to the MMW frequency, filtered, amplified and the 27.5 GHz signals introduced into the chamber using horn antennas. Three metal model stirrers per chamber were used to maximize field scattering and therefore its homogeneity. A number of upconverter power amplifier chains were used to generate sufficient MMW power to achieve the required field strengths. Each chamber was equipped with two EY-V4 isotropic MMW field probes (SPEAG, Switzerland) to monitor the exposure fields, the MMW power was then adjusted to maintain the target field strength within each. Each chamber was designed to accommodate up to 12 cages (surface area per cage 501 cm^2). Ventilation was ensured via honeycomb ventilation panels, and the 12-hour light/dark cycle was guaranteed by a lighting system of LED strips (95 ± 2 lux). The field and environmental parameters have been monitored and recorded continuously (sample time of 10 s). Bedding (500 gr) has been checked daily and changed once a week; food was weighed (35 gr) and supplied directly into the cage on a daily basis.

Mice and tissue collection

CD1 females were mated with males lacking one *Ptch1* allele (CD1.129-Ptch1tm1Zim/Enea; named $Ptch1^{+/-}$ throughout the text). To avoid disturbances to the magnetic and electric fields, each litter, along with its mother, was housed in cages made entirely of polycarbonate with drinking bottles specifically designed with glass sipper tubes. Importantly, the same cages used for mating and gestation were directly placed inside the exposure chambers at P1. This procedure was specifically implemented to minimize potential maternal stress linked to environmental change.

Thus, litters were randomly assigned to one of three electromagnetic reverberation chambers (for each experimental group, four cages were used; each litter consisted of 12 pups) and whole-body exposed until weaning (P21) at 27.5 GHz, 10 min on and 5 min off, for 23 h per day. Throughout the entire duration of the exposure, mice were routinely examined for general health status once a day.

At the end of the exposure, offspring were genotyped as previously described by[4]. The biological analysis on the collected samples has been conducted using blind protocols: at the end of the exposure period, an alphanumeric code has been assigned by the operators identified at the start of the experiment who have not been involved in the subsequent biological analysis phase, hence maintaining the blinding.

Mice were euthanized by cervical dislocation at 21 days of age (average body weight: 9.73 ± 1.33 g). Death was verified by confirming the absence of reflexes, respiratory activity, and cardiac function. From each mouse, samples of dorsal skin were fixed in 4% formaldehyde for histological analysis or snap-frozen for molecular analysis. Maternal skin was not included in this study to avoid confounding factors related to the stress of lactation. This animal study was performed according to the European Community Council Directive 2010/63/EU, approved by the local Ethical Committee for Animal Experiments of the ENEA, and authorized by the Italian Ministry of Health (n° 107/2023-PR). All animal experiments were conducted in accordance with the ARRIVE guidelines.

Histological, morphometric, and immunohistochemical analysis of skin

Skin sample collection and preparation

Dorsal skin was harvested from WT and $Ptch1^{+}$ mice at postnatal day 21 following 5G exposure. Prior to sample collection, the dorsal hair coat was shaved to ensure uniform hair regrowth. Skin samples were then processed for histology by standard techniques. Briefly, tissues were fixed in 4% neutral-buffered formaldehyde dehydrated through a graded ethanol series, cleared in xylene, and embedded in paraffin. From each paraffin block, 4 µm-thick sections were cut using a rotary microtome and mounted on glass slides. For routine histological evaluation, sections were dewaxed in xylene, rehydrated through decreasing concentrations of ethanol, and stained with hematoxylin and eosin (H&E). After staining, slides were dehydrated, cleared, and coverslipped for microscopic examination.

Morphometric analysis

Skin morphometric analyses were performed to evaluate the epidermal thickness, as well as the density and depth of hair follicles. For these analyses, animals with the correct histological orientation of skin were selected to ensure accurate measurements and to avoid bias ($n = 6$ animals per experimental group for each genotype). Five non-overlapping fields per animal were analyzed at 10× magnification (each field ≈ 850 µm; total analyzed length ≈ 4.2 mm per animal). Within each field, five independent measurements of epidermal thickness (µm) were obtained. Hair follicles were manually counted in the same fields, and follicle density was expressed as the number of follicles per millimeter of skin (n/mm). Hair follicle depth (µm) was measured in the same regions and used as an indicator of follicular activity and skin regenerative status. For each parameter, mean values were calculated per animal and subsequently across experimental groups.

F4/80 immunohistochemistry

Four-micron sections of paraffin-embedded skin were prepared to evaluate inflammatory infiltration. Sections underwent heat-mediated antigen retrieval (HMARS, Abcam, Germany), were washed in water, and endogenous peroxidase activity was blocked with 3% H_2O_2 for 10 min. Non-specific binding was minimized by incubation with 5% bovine serum albumin in PBS for 20 min.

Sections were then incubated overnight at 4 °C with a primary antibody against F4/80 (Abcam, UK; 1:500), a macrophage marker, followed by incubation with an anti-rabbit secondary antibody (Abcam, UK; 1:200). The antigen–antibody reaction was visualized using a DAB detection kit (Dako, USA), and sections were counterstained with hematoxylin.

F4/80-positive areas were quantified using HistoQuest software (TissueGnostics, Austria). Macrophage density was calculated as F4/80-positive area (μm²) normalized to the total analyzed tissue area. Nuclear counterstaining was used to ensure accurate identification of macrophages within the dermal compartment. To eliminate run-to-run technical staining variability, data were expressed as fold change relative to the respective SHAM controls. A total of 12 animals per experimental group for each genotype were analyzed.

Mast cell analysis

Mast cell degranulation was assessed on 5 μm sections stained with Toluidine Blue (Bio-Optica, Italy). Sections were dewaxed, rehydrated through graded ethanol (100%, 95%, 70%) to distilled water, stained for 2 min at room temperature, briefly differentiated in 96% ethanol (5 s), dehydrated, cleared, and mounted with synthetic resin. For each animal (12 animal each experimental group for each genotype), seven frames per Sects. (700,000 μm², 20× magnification) were analyzed using NIS-Elements BR 5.30.01 software (Nikon Instruments, Italy). Results were expressed as total mast cells per mm² and as the percentage of degranulated mast cells relative to the total mast cell count.

RT2 profiler PCR array on genes of mouse inflammatory cytokines & receptors

Total RNA was isolated from dorsal skin tissues of *Ptch1*$^{+/-}$ mouse using the RNeasy Microarray tissue kit (QIAGEN Hilden, Germany), and 500 ng of total RNA was reverse transcribed by the RT2 First Strand Kit (QIAGEN). cDNA samples - three pools of three animals each (biological replicates) for each sex, were analyzed by a RT2 Profiler PCR array (Gene GlobeID: PAMM-011Z, QIAGEN) to analyse the expression levels of 84 crucial genes regulating the inflammatory process amplified by RT^2 SYBR Green qPCR Mastermix (QIAGEN). Gene list: *Chemokines: Ccl1* (*I-309*), *Ccl11* (*Eotaxin*), *Ccl12* (*MCP-5*, *Scya12*), *Ccl17* (*Tarc*), *Ccl19*, *Ccl2* (*MCP-1)Ccl20* (*Mip-3a*), *Ccl22* (*Mdc*), *Ccl24* (*Mpif-2*, *Eotaxin-2*), *Ccl3* (*Mip-1a*), *Ccl4* (*Mip-1b*), *Ccl5* (*Rantes*), *Ccl6*, *Ccl7* (*Mcp3*), *Ccl8* (*Mcp2*), *Ccl9*, *Cx3cl1*, *Cxcl1* (*Gro1*), *Cxcl10* (*Inp10*), *Cxcl11* (*Itac*, *Ip9*), *Cxcl12*, *Cxcl13*, *Cxcl15*, *Cxcl5* (*ENA-78*, *LIX*), *Cxcl9* (*Mig*); *Chemokine Receptors: Ccr1*, *Ccr10*, *Ccr2*, *Ccr3*, *Ccr4*, *Ccr5*, *Ccr6*, *Ccr8*, *Cxcr2*, *Cxcr3*, *Cxcr5*; *Interleukins: Il11*, *Il13*, *Il15*, *Il16*, *Il17a*, *Il17b*, *Il17f*, *Il1a*, *Il1b*, *Il1rn*, *Il21*, *Il27*, *Il3*, *Il33*, *Il4*, *Il5*, *Il7*; *Interleukin Receptors: Il10ra*, *Il10rb*, *Il1r1*, *Il2rb*, *Il2rg*, *Il5ra* (*Cd125*), *Il6ra*, *Il6st* (*Gp130*); *Other Cytokines: Aimp1*, *Bmp2*, *Cd40lg*, *Csf1* (*Mcsf*), *Csf2* (*GMCSF*), *Csf3* (*Gcsf*), *Fasl*, *Ifng*, *Lta* (*Tnfb*), *Ltb*, *Mif*, *Nampt*, *Osm*, *Pf4*, *Spp1*, *Tnf*, *Tnfsf10* (*Trail*), *Tnfsf11* (*Rankl*), *Tnfsf13*, *Tnfsf13b*, *Tnfsf4* (*Ox40l*), *Vegfa*; *Other Cytokine Receptors: Tnfrsf11b* (*Opg*) (RT2 Profiler PCR Array Handbook, QIAGEN). Normalization and all data analyses were performed according to the manufacturer's instructions using their web-based software package:https://dataanalysis.QIAGEN.com/pcr/arrayanalysis.

For the normalization, it uses the average of five housekeeping genes: *Actb*, *B2m*, *Gapdh*, *Gusb*, *Hsp90ab1*. To identify false positives, a statistical assessment of the False Discovery Rate was carried out by Benjamini–Hochberg procedure with the critical value of 0.05 (http://www.biostathandbook.com/multiplecomparisons.html).

Network analysis

Cytoscape 3.10.2 (UC, San Diego, California, USA) was used to identify potential correlations between the differentially expressed genes identified with the RT2 Profiler PCR Array with a cutoff of ≥ 2-fold regulation and p-value < 0.05. A confidence score ≥ 0.4 and a maximum number of additional interactors = 0 were set as the STRING cutoff criterion.

Gene Ontology (GO) Enrichment Analysis has been performed with the online tool on https://geneontology.org/ (accessed on 11–16/12/2024), with a PANTHER Overrepresentation Test (Released 2024-08-07) on Reactome database (version 86 Released 2023-09-07).

Results are plotted using the Enrichment bubble plot from SRPLOT (https://www.bioinformatics.com.cn/).

Real time (RT)-PCR

Total RNA was isolated from mouse dorsal skin of all mice in experiment (both CD1 and *Ptch1*$^{+/-}$) using the mini-RNeasy kit (# 74104, QIAGEN), and 1 μg of total RNA was reverse transcribed by High-Capacity cDNA Reverse Transcription Kit (Applied Biosystems, Foster City, CA, USA). The RT-PCR amplifications were obtained by a StepOnePlus Real-Time PCR Detection System using Power up SYBR Green Master Mix (Applied Biosystems). Reactions were performed in triplicate from each biological replicate. *Glyceraldehyde-3-phosphate dehydrogenase* (*Gapdh)* or *B2-microtubulin* (*B2m)* were used as house-keeping genes for normalization. The ΔΔCt quantitative method was used to normalize expression of the reference gene and to calculate the relative expression levels of target genes. The murine primers used are summarized in Supplementary Table 1.

Glutamate quantification

Cutaneous glutamate levels were quantified using the bioluminescent Glutamate-Glo™ Assay (Promega, Madison, WI, USA; Cat. #J1611), following the manufacturer's instructions for tissue metabolites. Briefly, dorsal skin biopsies (~ 5 mg) collected at P21 were snap-frozen in liquid nitrogen and stored at −80 °C. For metabolite extraction, frozen samples were accurately weighed and homogenized in a mixture of Tris-HCl homogenization buffer (50 mM, pH 7.5) and inactivation buffer (0.6 N HCl) using a mechanical tissue disruptor (gentleMACS™ Dissociator; Miltenyi Biotec, Bergisch Gladbach, Germany). The addition of 0.6 N HCl during homogenization ensured immediate enzyme inactivation and metabolic stabilization by deproteinizing the samples. The resulting lysates were centrifuged at 13,000 r.p.m. for 5 min at 4 °C to remove cellular debris. Supernatants were carefully collected and neutralized by the addition of 0.5 M Tris-base buffer to reach a physiological pH. Neutralized aliquots (50 μl) were then transferred to 96-well white plates and incubated with the Glutamate Detection Reagent for 1 h at room temperature. Luminescence was recorded using a GloMax® Multi Detection System

(Promega). Final glutamate concentrations were normalized to the initial biopsy weight, and expressed as μM/mg of tissue.

Statistics

Data are presented as mean ± SEM. Statistical tests appropriate for samples distribution and group comparisons were applied using GraphPad Prism (GraphPad Software, San Diego, CA, USA). Normal distribution and homogeneity of variance were assessed to determine the appropriate statistical tests. For multiple group comparisons where data followed a non-normal distribution, a non-parametric one-way ANOVA (Kruskal–Wallis test) was employed. For pairwise comparisons between the SHAM control and experimental groups within each genotype, an unpaired Student's t-test with Welch's correction was applied when the assumption of equal variances was not met. For histological analyses, where sample sizes were smaller compared to molecular and biochemical datasets, pairwise comparisons were performed using the Mann–Whitney U test. Differences were noted as significant * $p < 0.05$, ** $p < 0.01$, *** $p < 0.001$, **** $p < 0.0001$.

Data availability

Data will be made available on request by contacting Mariateresa Mancuso, mariateresa.mancuso@enea.it.

Received: 22 September 2025; Accepted: 5 June 2026
Published online: 08 June 2026

References

1. Di Ciaula, A. Towards 5G communication systems: Are there health implications? *Int. J. Hyg. Environ. Health*. **221**, 367–375 (2018).
2. Russell, C. L. 5G wireless telecommunications expansion: Public health and environmental implications. *Environ. Res.* **165**, 484–495 (2018).
3. Leszczynski, D. Physiological effects of millimeter-waves on skin and skin cells: an overview of the to-date published studies. *Rev. Environ. Health*. **35**, 493–515 (2020).
4. Pazzaglia, S. Ptc1 heterozygous knockout mice as a model of multi-organ tumorigenesis. *Cancer Lett.* **234**, 124–134 (2006).
5. Aszterbaum, M. et al. Ultraviolet and ionizing radiation enhance the growth of BCCs and trichoblastomas in patched heterozygous knockout mice. *Nat. Med.* **5**, 1285–1291 (1999).
6. Mancuso, M. et al. Basal cell carcinoma and its development: insights from radiation-induced tumors in Ptch1-deficient mice. *Cancer Res.* **64**, 934–941 (2004).
7. Mancuso, M. et al. Hair cycle-dependent basal cell carcinoma tumorigenesis in Ptc1neo67/+ mice exposed to radiation. *Cancer Res.* **66**, 6606–6614 (2006).
8. Jain, A. et al. Nociceptor-immune interactomes reveal insult-specific immune signatures of pain. *Nat. Immunol.* **25**, 1296–1305 (2024).
9. Hakimet, S., Jain, A. & Woolf, C. J. Immune drivers of pain resolution and protection. *Nat. Immunol.* **25**, 2200–2208 (2024).
10. Yang, J. X. et al. Potential Neuroimmune Interaction in Chronic Pain: A Review on Immune Cells in Peripheral and Central Sensitization. *Front. Pain Res. (Lausanne)*. **3**, 946846 (2022).
11. Zhang, S. et al. Nonpeptidergic neurons suppress mast cells via glutamate to maintain skin homeostasis. *Cell* **184** (8), 2151–2166e16 (2021).
12. Zhang, Y. R. et al. Agonism of the glutamate receptor GluK2 suppresses dermal mast cell activation and cutaneous inflammation. *Sci. Transl Med.* **16** (777), eadq9133 (2024).
13. Iakovidis, S. et al. Murine Skin Dosimetry Under Millimeter Wave Exposure. *IEEE J. Microw.* **4**, 204–202 (2024).
14. Chilukoti, N., Pavuluri, S. & Kumar, S. Differential expression of keratin and keratin associated proteins are linked with hair loss condition in spontaneously mutated inbred mice. *Biochem. Biophys. Res. Commun.* **741**, 151032 (2024).
15. Meixiong, J., Basso, L. & Dong, X. Gaudenzio, N. Nociceptor-Mast Cell Sensory Clusters as Regulators of Skin Homeostasis. *Trends Neurosci.* **43**, 130–132 (2020).
16. Yang, B. G. et al. Degranulation of Mast Cells as a Target for Drug Development. *Cells* **12**, 1506 (2023).
17. International Commission on Non-Ionizing Radiation Protection (ICNIRP). Guidelines for Limiting Exposure to Electromagnetic Fields (100 kHz to 300 GHz). *Health Phys.* **118**, 483–524 (2020).
18. Gandhi, O. P. & Riazi, A. Absorption of Millimeter Waves by Human Beings and Its Biological Implications. *IEEE Trans. Microw. Theory Techn*. **34**, 228–235 (1986).
19. Wood, A., Mate, R. & Karipidis, K. Meta-analysis of in vitro and in vivo studies of the biological effects of low-level millimetre waves. *J. Expo. Sci. Environ. Epidemiol.* **31**, 606–613 (2021).
20. Scientific Committee on Emerging Newly Identified Health Risks. Opinion on potential health effects of exposure to electromagnetic fields. *Bioelectromagnetics* **36**, 480–484 (2015).
21. Forsyth, K. S., Jiwrajka, N., Lovell, C. D., Toothacre, N. E. & Anguera, M. C. The conneXion between sex and immune responses. *Nat. Rev. Immunol.* **24** (7), 487–502 (2024).
22. Araújo, M., Mendes-Frias, A. & Silvestre, R. Sex differences in immune modulation: implications for infection, inflammation, and nutritional supplementation. *Biol. Sex. Differ.* https://doi.org/10.1186/s13293-026-00857-1 (2026).
23. Martin-Vega, A. & Cobb, M. H. Navigating the ERK1/2 MAPK Cascade. *Biomolecules* **13**, 1555 (2023).
24. Munshi, A. & Ramesh, R. Mitogen-activated protein kinases and their role in radiation response. *Genes Cancer*. **4**, 401–408 (2013).
25. Chelombitko, M. A., Fedorov, A. V., Ilyinskaya, O. P. & Zinovkin, R. Role of reactive oxygen species in mast cell degranulation. *Biochemistry (Mosc)* **81**, 1564–1577 (2016).
26. Miyazaki, D. et al. Macrophage inflammatory protein–1α as a costimulatory signal for mast cell–mediated immediate hypersensitivity reactions. *J Clin Invest* **115**, 434–442 (2005).
27. Frandji, P. et al. Presentation of soluble antigens by mast cells: Upregulation by interleukin-4 and granulocyte/macrophage colony-stimulating factor and downregulation by interferon-gamma. *Cell Immunol* **163**, 37–46 (1995).
28. Shi, Y. et al. Granulocyte-macrophage colony-stimulating factor (GM-CSF) and T-cell responses: What we do and don't know. *Cell Res* **16**, 126–133 (2006).
29. Singh, J., Shah, R. & Singh, D. Targeting mast cells: Uncovering prolific therapeutic role in myriad diseases. *Int Immunopharmacol* **40**, 362–384 (2016).
30. Lim, J. H. et al. RANKL down-regulates the mast cell proliferation through inducing senescence. *Cytokine* **159**, 156018 (2022).
31. Theoharides, T. C., Tsilioni, I. & Ren, H. Recent advances in our understanding of mast cell activation - or should it be mast cell mediator disorders?. *Expert Rev Clin Immunol* **15**, 639–656 (2019).

32. Gómez-Aleza, C. et al. Inhibition of RANK signaling in breast cancer induces an anti-tumor immune response orchestrated by CD8+ T cells. *Nature Communications* **11**6335, 6335. (2020).
33. Liu, J., Jia, S., Huang, F., He, H. & Fan,. Peripheral role of glutamate in orofacial pain. *Front. Neurosci.* **929136**, 929136. https://doi.org/10.3389/fnins.2022.929136 (2022).
34. Denda, M. & Elias, P. M. Review of sensory systems deployed by epidermal keratinocytes. *Frontiers in Cell and Developmental Biology* **13**, 1598326. https://doi.org/10.3389/fcell.2025.1598326 (2025).
35. Gujar, A., Sharma, S., Verma, R. & Singh,. Nerve growth factor signaling regulates glutamate production and neurogenic inflammation. *International Journal of Molecular Sciences* **6053**, 6053. https://doi.org/10.3390/ijms25116053 (2024).
36. Davis,. Homeostatic signaling and the stabilization of neural function. *Neuron* **728**, 718–728. https://doi.org/10.1016/j.neuron.2013.09.044 (2013).
37. Rathore, A. P. S. & Ginhoux,. New perspectives on the origins and heterogeneity of mast cells. *Nat Rev Immunol.* **68**, 55–68 (2023).

Acknowledgements

We thank Monica Serra and Mirko Romano for their excellent assistance with mouse handling and their support during the experiments.

Author contributions

Conceptualization: MM; Data curation: FP, EF, MM; Formal analysis: FP, EF; Funding acquisition: TS; Investigation: FP, EF, FN, SL, IDS, EP, MT, RP, LA, AZ, FC, MP, CM, SP, MC; Methodology: FN, SL, IDS, EP, MT, RP, LA, AZ, FC, MP, CM, SP; Resources: MM; Supervision: MM; Writing – original draft: FP, EF; Writing – review & editing: MC, MM.

Funding

This project received funding from the European Union's Horizon Europe Framework Programme under Grant Agreement number 101057622 (SEAWave Project).

Declarations

Competing interests

The authors declare no competing interests.

Additional information

Supplementary Information The online version contains supplementary material available at https://doi.org/10.1038/s41598-026-57133-w.

Correspondence and requests for materials should be addressed to M.M.

Reprints and permissions information is available at www.nature.com/reprints.

Publisher's note Springer Nature remains neutral with regard to jurisdictional claims in published maps and institutional affiliations.

Open Access This article is licensed under a Creative Commons Attribution-NonCommercial-NoDerivatives 4.0 International License, which permits any non-commercial use, sharing, distribution and reproduction in any medium or format, as long as you give appropriate credit to the original author(s) and the source, provide a link to the Creative Commons licence, and indicate if you modified the licensed material. You do not have permission under this licence to share adapted material derived from this article or parts of it. The images or other third party material in this article are included in the article's Creative Commons licence, unless indicated otherwise in a credit line to the material. If material is not included in the article's Creative Commons licence and your intended use is not permitted by statutory regulation or exceeds the permitted use, you will need to obtain permission directly from the copyright holder. To view a copy of this licence, visit http://creativecommons.org/licenses/by-nc-nd/4.0/.

© The Author(s) 2026